Bulk critical state and fundamental length scales of superconducting nanocrystalline Nb_3Al in Nb-Al matrix

Puspen Mondal,[1] Meghmalhar Manekar,[1,*] A. K. Srivastava,[2] and S. B. Roy[1]
[1]*Magnetic and Superconducting Materials Section, Raja Ramanna Centre for Advanced Technology, Indore 452 013, India*
[2]*Indus Synchrotrons Utilisation Division, Raja Ramanna Centre for Advanced Technology, Indore 452 013, India*
(Received 9 April 2009; revised manuscript received 21 May 2009; published 1 July 2009)

We present the results of magnetization measurements on an as-cast nanocrystalline Nb_3Al superconductor embedded in Nb-Al matrix. The typical grain size of Nb_3Al ranges from about 2–8 nm with the maximum number of grains at around 3.5 nm, as visualized using transmission electron microscopy. The isothermal magnetization hysteresis loops in the superconducting state can be reasonably fitted within the well-known Kim-Anderson critical-state model. By using the same fitting parameters, we calculate the variation in field with respect to distance inside the sample and show the existence of a critical state over length scales much larger than the typical size of the superconducting grains. Our results indicate that a bulk critical current is possible in a system comprising of nanoparticles. The nonsuperconducting Nb-Al matrix thus appears to play a major role in the bulk current flow through the sample. The superconducting coherence length ξ is estimated to be around 3 nm, which is comparable to the typical grain size. The penetration depth λ is estimated to be about 94 nm, which is much larger than the largest of the superconducting grains. Our results could be useful for tuning the current carrying capability of conductors made out of composite materials which involve superconducting nanoparticles.

DOI: 10.1103/PhysRevB.80.024502 PACS number(s): 74.78.Na, 74.81.Bd, 74.25.Sv, 74.70.Ad

I. INTRODUCTION

Nanocrystalline superconductors provide an interesting situation where the fundamental length scale, the coherence length ξ, is comparable to the sample dimensions. Some studies of superconducting properties have been carried out on artificially grown In,[1] Nb,[2] Al,[3,4] and $PbMo_6S_8$ (Ref. 5) nanoparticles. The decrease in the particle size of $PbMo_6S_8$ in the range of few tens of nanometres resulted in a dramatic increase in the upper critical field, presumably due to the decrease in coherence length.[5] On the other hand, it has been observed, through tunneling experiments on single isolated Al nanoparticles, that superconductivity ceases to exist when the grain size is reduced to the order of $\sim 5-10$ nm.[4] This vanishing of superconductivity was shown to occur because the spacing between the electronic energy levels exceeds the superconducting energy gap in bulk material.[4,6] Further studies on superconducting nanowires showed that as the wire thickness is decreased to the order of ξ, the transition to the low-temperature state from the room-temperature state becomes a dissipative phase transition.[6,7] These studies[4,6,7] show that a flow of dissipationless current is not possible in case of particles which are nearly of the size of the coherence length,[7] a limit posed by the nature of the phase ϕ of the superconducting wave function.

In a recent work on the composite system of nanocrystalline Nb_3Al embedded in Nb-Al solid solution matrix,[8] we have shown that the thermomagnetic history effects in nanosized superconductors could be quite different compared to those seen in bulk superconductors, an information quite useful for understanding the flux-pinning properties of such composites. We have shown[8] that though the temperature-dependent magnetization shows a distinct irreversibility during the zero-field-cooled (ZFC) and the field-cooled-cooling (FCC) measurements such as in bulk superconductors, the field-cooled-warming (FCW) curve coincides with the FCC curve unlike the case of bulk superconductors with flux pinning. The thermal hysteresis between the FCC and FCW magnetization curves in bulk superconductors arises due to the freezing of flux front beyond the flux trapping depth L from the sample surface,[9] which leads to different field profiles inside the sample during the cooling and warming cycles. We had conjectured that in our case of nanocrystalline Nb_3Al, the flux trapping depth is probably much larger than the typical size of the superconducting grains, which may give rise to identical field profiles during the cooling and warming cycles and thus reversible FCC and FCW curves.[8]

In this work we show that a bulk critical (dissipationless) current is possible in the present case of very small self-assembled superconducting nanoparticles of Nb_3Al (sizes on the order of ξ) which are separated by a nonsuperconducting matrix. This observation is contrary to the earlier works on superconducting nanoparticles and nanowires.[4,6,7] In the present composite system discussed here, the nonsuperconducting matrix is essentially metallic in nature and is in close contact with the superconducting grains. Whereas, the nonsuperconducting surroundings of isolated Al nanoparticles (Ref. 4) are made of a very-high-resistance substrate of Si_3N_4 in two of the dimensions and vacuum in the third, which does not allow the coupling of superconducting wave function of the Al particles across the barrier. In our composite system, the combined effect of the nanosized superconducting grains and the normal (metallic) matrix results in a bulklike superconducting response from the sample for the flow of electrical current. We analyze the isothermal magnetization hysteresis loops in the superconducting state in terms of the well-known Kim-Anderson critical-state model. The flux profiles inside the superconductor calculated from the same fitting parameters show a field variation over length

scales much larger than the typical length scales of the superconducting grains, which indicates that a bulk critical state is possible in this composite system made of nanoparticles. The fundamental length scales of a superconductor, the penetration depth λ, and the coherence length ξ for our sample are also compared with the grain size. We find that while ξ is comparable to the typical grain size, λ is much larger than the size of the superconducting grains.

Superconducting properties in Nb_3Al nanoparticles prepared by gas-condensation method have been studied earlier.[10] The authors have observed that superconductivity vanishes if the grain size is below 15 nm,[10] an observation very similar to the case of Al nanoparticles.[4,6] Our results presented here on much smaller nanoparticles (2–8 nm) thus further emphasize the important role of the nonsuperconducting matrix for the possibility of superconductivity at such small length scales. These results can provide further insight into tuning the properties of nonsuperconducting matrix to enable interesting applications such as current-carrying superconducting nanoparticles and nanowires.

II. EXPERIMENTAL

Nb_3Al (~1 gm mass) was prepared by arc melting the constituent elements taken in stoichiometric proportions. The sample was not subjected to any further heat treatment. The details of sample characterization using x-ray diffraction (XRD) are mentioned in our earlier report.[8] For further characterization of the sample, especially for visualizing the nanoparticles, a small piece of the sample was cut from the same parent button for transmission-electron-microscopy (TEM) studies. A commercial TEM (Phillips, CM200) with a LaB_6 filament as cathode was used at an accelerating anode voltage of 200 kV. Magnetization (M) measurements were performed as a function of field (H) and temperature (T) using a commercial vibrating sample magnetometer (Quantum Design). The sample for this purpose was obtained from the same parent button in form of a rectangular slab of $2.73 \times 0.72 \times 0.38$ mm^3 size. The demagnetization factor for this geometry with H parallel to the long axis is 0.1133.[11] For measuring the isothermal magnetization, the external field was swept at a rate of 100 Oe/s.

III. RESULTS AND DISCUSSION

Figure 1(a) shows the dark field TEM image of the sample. The diffraction pattern [Fig. 1(b)] indicates the polycrystalline nature of the sample. The dark field micrograph [Fig. 1(a)] corresponds to the Nb_3Al grains which are oriented along [211]. The grain-size distribution calculated from Fig. 1(a) has a peak at about 3.5 nm and the largest grains are of nearly 9 nm [Fig. 1(c)]. In our earlier work we had estimated the average grain size to be around 35 nm through a preliminary analysis of the XRD peaks,[8] which did not include the effect of strain and dislocations on the peak widths. This could be the reason for the apparent mismatch between the results of TEM and the inference from XRD pattern. The analysis of the structural properties of nanocrystalline Nb_3Al using both XRD and TEM will be a part of our future work and will be communicated separately. The dark regions in Fig. 1(a) are grains of both the Nb_3Al phase at an orientation different from the [211] direction and the randomly oriented grains of the Nb-Al solid solution. The crystalline nature of the Nb-Al phase has been seen in the XRD pattern.[8] There is also an amorphous phase (most probably of Nb-Al) between the grains [see Fig. 1(a)] which indicates that the microstructure of the sample corresponds to very early stages of nucleation of the Nb_3Al phase. The lattice constant of Nb_3Al is about 5.2 Å (Ref. 12) which means that most of our sample consists of grains which are only of 6–8 unit cells. The formation of Nb_3Al phase is possible only when the cooling from melt occurs at an extremely high rate of almost 10^4 K/s.[12] Probably such high cooling rate could be achieved in our arc-melting furnace due to the very small mass of the sample. The rapidly quenched melt almost always results in a composite system of Nb_3Al grains embedded in Nb-Al solid solution, due to the complex phase diagram of the Nb-Al binary system.[12,13] Further growth of the Nb_3Al grains can be achieved by prolonged annealing of the composite system at lower temperature, which transforms the Nb-Al solid solution to the stable Nb_3Al phase.[12,13] Our sample was studied in the as-cast condition and was not subjected to any heat-treatment schedules after the initial solidification, which has thus resulted in a composite system. The presence of very small grains embedded in an amorphous matrix indicates that the crystalline phase did not receive sufficient time for further growth.

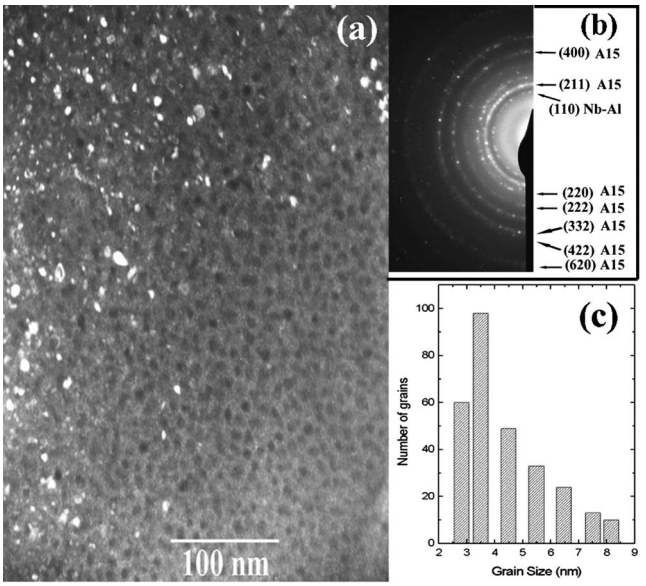

FIG. 1. Results of TEM measurements. (a) Dark field image of the sample on a submicron scale. See text for details. (b) Diffraction pattern of the sample indexed for the A15 structure of the Nb_3Al phase. (c) Grain-size distribution in a nearby location of the sample shown in (a).

The piece of sample used for TEM cannot be used for magnetization measurements. Hence it is necessary to establish the equivalence of different pieces of the same sample button. Randomly chosen pieces for XRD from different locations of the parent sample (which were not used for TEM) also confirmed the nanocrystalline nature of the Nb_3Al em-

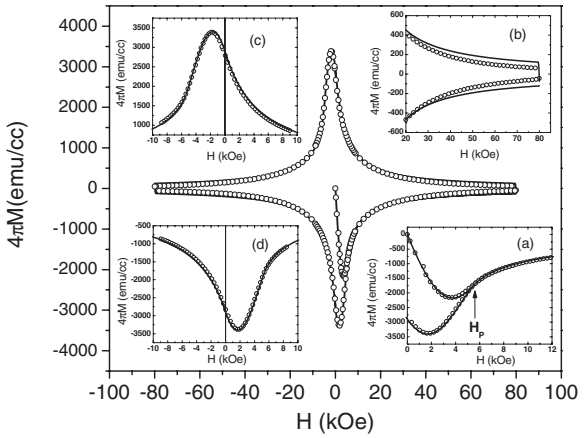

FIG. 2. Isothermal *M-H* curve at 4 K. The open circles are experimental data points and the solid lines are calculated curves using the Kim-Anderson model. See text for the details of calculation. Inset (a) shows the expanded view in the fourth quadrant at low fields. Inset (b) shows the expanded region at high fields in the fourth and first quadrants. Inset (c) shows the low-field region in the first and second quadrants. Inset (d) shows the low-field region in the third and fourth quadrants.

bedded in Nb-Al matrix.[8] The microstructure in TEM measurements was observed at various locations over a span of about 0.7 mm, which is comparable to one of the dimensions of the piece used for magnetization. The morphology was found to be nearly similar at all these locations, out of which a representative location is shown in Fig. 1. Magnetization measurements on different pieces of the sample at distant locations on the parent button yielded the same transition temperature T_C and nearly identical isothermal *M-H* curves.

With this detailed characterization of the sample, we now study its superconducting properties. Figure 2 shows *M* as a function of *H* at $T=4$ K. At this temperature, the Nb-Al phase is not in the superconducting state.[8] The measurements are performed in the ZFC state. In the ZFC protocol, the sample is first cooled in zero field from $T=30$ K down to $T=4$ K. *M* is then measured while increasing *H* isothermally up to 80 kOe. A large hysteresis in *M* is observed on reducing the field, which indicates the presence of a critical state in the superconducting phase. This hysteresis loop is completed for all four quadrants after the virgin cycle. For fitting the experimental *M-H* hysteresis curve, we use the well-known Kim-Anderson model of critical state where the critical current density J_C is given by

$$J_C(H_i) = \frac{10}{4\pi}\frac{k}{(H_0 + H_i)}, \tag{1}$$

where k and H_0 are constants, which are treated as fitting parameters and H_i is the internal field. Here we have chosen the units such that J_C is in A cm^{-2}, k is in Oe^2 cm^{-1}, and H_0 and H_i are in Oe. With these units, $4\pi M$ is taken as volume magnetization (emu/cc) to give dimensionless susceptibility which makes the calculation of the *M-H* curves easier.

The complete solution of Eq. (1) for calculating the *M-H* curves for an orthorhombic (parallelopiped) geometry is given by Chen and Goldfarb.[14] Here we use the same equations for fitting our experimental *M-H* curves. While Chen and Goldfarb[14] have provided a complete solution for various cases, only some of the equations (with the same notations) which are applicable to our case are reproduced here for the sake of continuity.

The equation for initial part of the virgin curve for field values less than the field for full penetration H_P (defined later) is given by

$$M(H) = -\frac{Hx_0(b-a+x_0)}{ab} - \frac{S_1(b+x_0)(a-x_0)}{ab} + (S_1^3 - H_0^3)Q_1 + 2\frac{H_0^3(a-x_0)}{5kab}, \tag{2}$$

where

$$S_1 = H_0 + H, \tag{3a}$$

$$Q_1 = \frac{5k(a+b) - 2S_1^2}{15abk^2}. \tag{3b}$$

"x_0" is the distance from the center of the sample up to which the field has penetrated and "a" and "b" are related to the sample dimensions. In our case, $2a=0.38$ mm and $2b=0.72$ mm.

Inset (a) of Fig. 2 shows the experimental virgin *M-H* curve at low fields along with the calculated curve using Eq. (2) (we shall discuss about the envelope curve later). The experimental plot of $4\pi M$ as a function of the demagnetization-factor-corrected *H* gives a slope of −1. The demagnetization factor was calculated for the entire bulk sample and not for the nanoparticle geometry. This clearly gives the first indication that the screening occurs as if the entire bulk is superconducting, instead of each individual nanoparticle of Nb_3Al which is separated by a matrix of crystalline and amorphous Nb-Al solid solution.

The other aspect to be noted about the calculated curve is that though the lower critical field H_{C1} is assumed to be zero in the model, the initial part of the virgin curve has a slope of −1, a surprising fact noticed by Chen and Goldfarb.[14]

The second segment of the virgin curve for field values greater than H_P up to the maximum field H_m (80 kOe in our case) is given by

$$M(H) = -S_1 + (S_1^3 - R_1^3)Q_1 + 2\frac{R_1^3}{5kb}, \tag{4}$$

where

$$R_1 = (S_1^2 - 2ka)^{1/2}. \tag{5}$$

The fit is reasonably good till $H \leq 20$ kOe, but at higher field values the calculated magnitude of *M* is larger than the experimentally obtained *M* [inset (b) of Fig. 2]. This indicates that the J_C in our sample decays faster at higher fields compared to the prediction of the Kim-Anderson model.

On reversing the direction of the field change from the maximum field H_m, the small portion of the return curve till the reverse full-penetration field H_{prh} is given by

$$M(H) = -S_1 - (S_1^3 - R_2^3)Q_2 + (R_2^3 - R_4^3)Q_3 + 2\frac{[(x_1 - a)R_2^3 + x_1 R_4^3]}{5kab}, \quad (6)$$

where

$$R_2 = [S_1^2 + 2k(a - x_1)]^{1/2}, \quad (7a)$$

with

$$x_1 = a - \frac{[(H_0 + H_m)^2 - (H_0 + H)^2]}{4k}, \quad (7b)$$

$$R_4 = (S_2^2 - 2ka)^{1/2}, \quad (7c)$$

with

$$S_2 = H_0 + H_m \quad (7d)$$

and

$$Q_2 = \frac{[5k(a+b) + 2S_1^2]}{15abk^2}, \quad (7e)$$

$$Q_3 = \frac{[10k(a+b) + 3S_1^2 - 7S_2^2]}{30abk^2}. \quad (7f)$$

Inset (b) of Fig. 2 shows the plot of Eq. (6) which is the small segment joining the negative M in the fourth quadrant with the positive M in the first quadrant.

The larger portion of the field-decreasing curve from H_{prh} to zero in the first quadrant is given by

$$M(H) = -S_1 - (S_1^3 - R_5^3)Q_2 - \frac{2R_5^3}{5kb}, \quad (8)$$

where

$$R_5 = (S_1^2 + 2ka)^{1/2}. \quad (9)$$

Once again this curve matches quite nicely for $H \leq 20$ kOe [inset (c) of Fig. 2] but gives an overestimated value of M at higher fields.

The field-decreasing curve in the second quadrant from zero to $-H_P$ is given by

$$M(H) = \frac{S_3(a - x_3)(b + x_3)}{ab} - \frac{S_1 x_3(b - a + x_3)}{ab} - (S_3^3 - H_0^3)Q_4 - (H_0^3 - R_6^3)Q_5 - 2\frac{[(a - x_3)H_0^3 + x_3 R_6^3]}{5kab}, \quad (10)$$

where

$$S_3 = H_0 - H, \quad (11a)$$

$$R_6 = (H_0^2 + 2kx_3)^{1/2}, \quad (11b)$$

and

$$x_3 = a - \frac{[(H_0 - H)^2 - H_0^2]}{2k}. \quad (11c)$$

The fit with Eq. (10) is quite good as can be seen from the inset (c) of Fig. 2.

The remaining portion of the M-H curve in the second quadrant from $-H_P$ to $-H_m$ is given by

$$M(H) = S_3 - (S_3^3 - R_7^3)Q_4 - \frac{2R_7^3}{5kb}, \quad (12)$$

where

$$R_7 = (S_3^2 - 2ka)^{1/2}. \quad (13)$$

Once again we see that the calculated M is higher than the experimentally measured M at higher fields, a situation quite similar to that shown in inset (b) of Fig. 2. The M-H curve in the third quadrant can be generated by just reversing the sign of M and H for the curve in the first quadrant. Similarly the curve in the fourth quadrant can be obtained from the curve in the second quadrant. Inset (d) of Fig. 2 shows the fit at low fields in the third and fourth quadrant.

We now analyze the situation in inset (a) of Fig. 2 where the envelope curve meets the virgin curve. Following the convention of Chen and Goldfarb,[14] the field for full penetration H_P is defined as that field value where the virgin curve meets the envelope curve in the fourth quadrant. Experimentally, this field value in our case is about 5960 Oe whereas the calculated H_P turns out to be about 5410 Oe. This is a very good agreement between the model and experiment. The values of the constants H_0 and k in Eq. (1) which give this reasonably good description of the complete M-H curve in Fig. 2 are 1600 Oe and 1.266×10^9 Oe^2 cm^{-1}, respectively.

The estimates of k and H_0 obtained by fitting the M-H curve in Fig. 2 can be verified by comparing the J_C calculated from Eq. (1) and the J_C obtained from the width of the magnetization hysteresis loop. The J_C for an orthorhombic geometry is calculated from the experimental data as[14]

$$J_C(H) = 10 \times \frac{\Delta M(H)}{[a(1 - a/3b)]}, \quad (14)$$

where $\Delta M(H)$ is the difference in M at a particular H during the isothermal field-increasing and field-decreasing cycle, while a and b are related to the sample dimensions as mentioned earlier. Figure 3 shows the comparison of the experimentally obtained J_C with the calculated one at $T = 4$ K. Here we can clearly see that the Kim-Anderson model applies quite well below $H = 30$ kOe, whereas the J_C at higher fields is slightly overestimated in this model. We get a reasonably high J_C of about 3×10^5 A cm^{-2} near zero field at 4 K which could be of use for technological applications. In our earlier report,[8] we had slightly underestimated the value of J_C as our analysis was quite preliminary. However, we have now followed a more rigorous approach in this work by carefully analyzing the complete M-H curve and obtained a better estimate of J_C.

Having shown the applicability of the Kim-Anderson model for our sample, we now proceed to calculate the field profiles inside the sample using the same values of k and H_0 mentioned earlier. The field profile for field-increasing case is given by

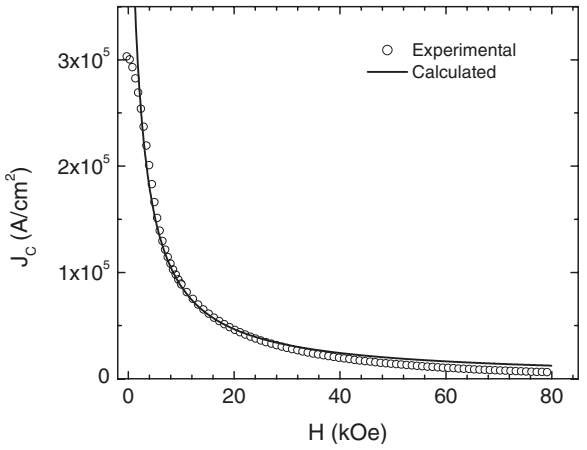

FIG. 3. Comparison of the calculated J_C from the Kim-Anderson model using the fitting parameters obtained by fitting the M-H curve in Fig. 2 and the experimentally obtained J_C at 4 K.

$$H_i = -H_0 + [2k(x-a) + (H_0+H)^2]^{1/2} \tag{15}$$

and the field profile for field-decreasing case is given by

$$H_i = -H_0 + [2k(a-x) + (H_0+H)^2]^{1/2}. \tag{16}$$

Figure 4 shows a few representative calculated field profiles for the actual sample dimensions. Curve "A" is for that applied field which is equal to the field for full penetration H_P. The value of H_P determined from the curve A and from the M-H curve in Fig. 2 turn out to be equal. This clearly shows that the critical state exists over the entire bulk sample instead of each nanoparticle of Nb_3Al. We emphasize here that at $T=4$ K, the Nb-Al phase is not superconducting and thus the particles of Nb_3Al are separated by a normal matrix. If the critical state was limited to only the nanocrystallites of Nb_3Al, the calculated value of H_P would have been completely different as the sample dimensions would have been a few nanometres instead of a fraction of millimeters. Curve "B" and "C" in Fig. 4 are for field values above and below

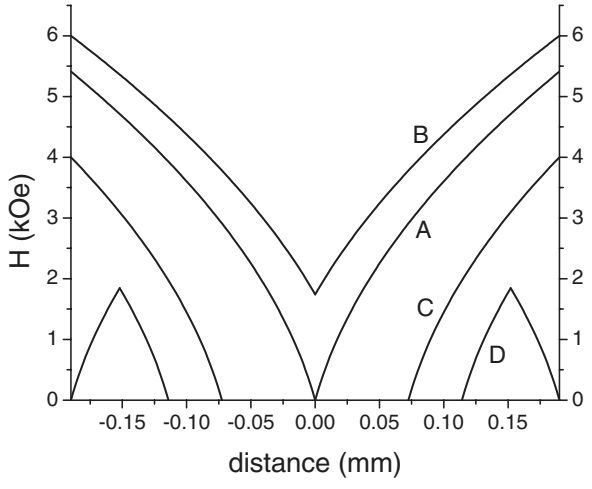

FIG. 4. Calculated field profiles at 4 K for the actual sample dimensions by using the same fitting parameters obtained from the calculated curve in Fig. 2.

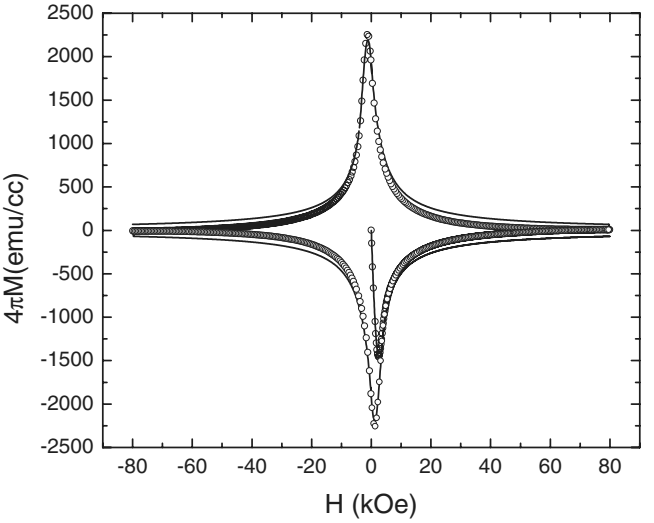

FIG. 5. Isothermal M-H curve at 8 K. Open circles are experimental data points while the solid line is the calculated curve from the Kim-Anderson model.

H_P, respectively. Curve "D" represents the remnant state where the field excursion was up to 3 kOe along the virgin curve. Curve D clearly shows a positive remnant magnetization (M_{rem}) which is expected in a bulk type-II superconductor in the presence of flux-pinning centers. We had shown such a positive M_{rem} in our earlier studies on the same sample.[8] It is thus quite clear that the typical length over which the field variation takes place inside the sample (hundreds of microns) is much greater than the characteristic length scale of the superconducting grains (few nanometres). This implies that the nonsuperconducting matrix, which consists of the Nb-Al solid solution, couples the superconducting Nb_3Al grains possibly through the proximity effect and plays an important role in establishing the bulk critical state in the sample. The profile of the local current density $J(x)$ inside the sample can be obtained by differentiating Eqs. (15) and (16) with respect to spatial coordinates. We however do not include those results here for conciseness.

Figure 5 shows the M-H curve at $T=8$ K. The experimental curve can be fitted with the Kim-Anderson model only for low fields. The experimentally measured M decreases much more rapidly at higher fields compared to the calculated magnitude of M. This indicates that the nonsuperconducting matrix is now less effective in carrying bulk current across the superconducting grains. At $T=8$ K, the Nb-Al phase is far above its superconducting transition temperature (3.8 K) (Ref. 8) and thus the current carrying capability of this phase can be easily reduced by application of relatively low fields. The values of the constants H_0 and k used for calculating the M-H curve at 8K are 1700 Oe and 0.7185×10^9 Oe^2 cm^{-1}, respectively.

Having studied the critical state in the sample, we now proceed to determine the H-T phase diagram in the superconducting state. The phase diagram is determined by performing T-dependent M measurements in various fields and also by H-dependent M measurements at various temperatures. Figure 6 shows one such isothermal M-H curve at $T=14$ K. From this curve it is quite difficult to determine the

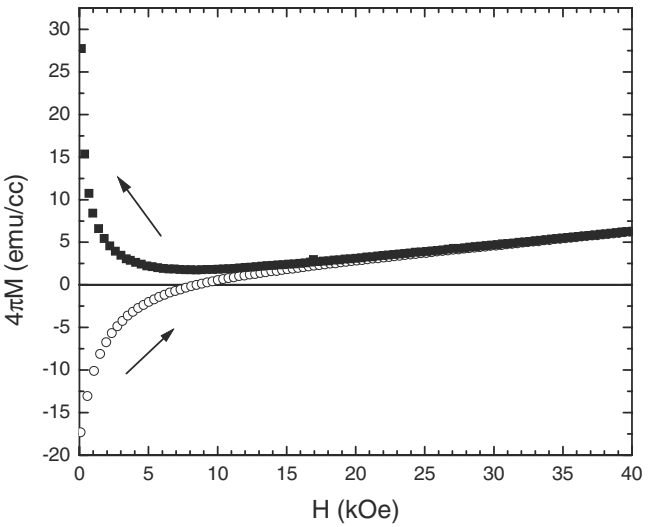

FIG. 6. Isothermal *M-H* curve at 14 K showing the presence of paramagnetic mixed state.

upper critical field (H_{C2}) as the mixed state clearly has a large paramagnetic susceptibility. Such large paramagnetic susceptibility has been reported in case of other A15 superconductors such as V_3Ga, V_3Si, and Nb_3Sn, which is thought to arise due to strong electron-electron correlations and the associated spin fluctuations.[15] We believe that Nb_3Al is also likely to have strong electron correlations in the normal state. Thus the determination of the boundary between the normal and superconducting phase has to be done by measuring the transition temperature T_C at various fields. However, the field irreversibility line $H_{irrv}(T)$ can be determined from the *M-H* curve as can be seen from Fig. 6.

The temperature irreversibility line $T_{irrv}(H)$ can be determined from the *M-T* curve where the FCC curve separates from the ZFC curve. Figure 7 shows the field- and temperature-irreversibility lines along with the $T_C(H)$ line which can be taken as the $H_{C2}(T)$ line, as it demarcates the normal and the superconducting regions in the *H-T* phase space. The $T_{irrv}(H)$ and the $H_{irrv}(T)$ lines do not coincide with each other. This could be because *T* and *H* were swept during the *M-T* and *M-H* measurements, respectively, instead of stabilizing at each data point. This indicates the metastable nature of the vortex state with the limits of metastability depending on the temperature or field sweep rate. The lower critical field (H_{C1}) is determined from the *M-H* curves at various temperatures by measuring the field at which the virgin curve deviates from a slope of −1. This gives the $H_{C1}(T)$ line which is shown as an inset to Fig. 7.

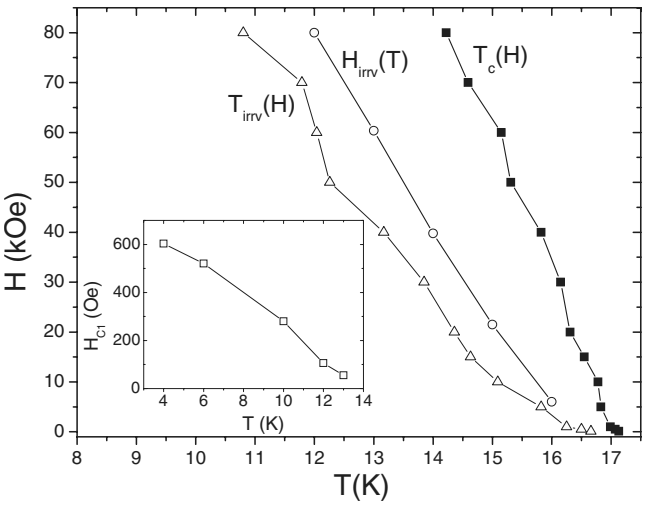

FIG. 7. *H-T* phase diagram determined from isothermal and temperature-dependent magnetization measurements. See text for details of the determination procedure. The lines are only a guide to the eyes and not any calculated curves. Inset shows the lower critical field as a function of temperature.

We now analyze the $H_{C2}(T)$ line in details to estimate the coherence length ξ at zero temperature. As seen from Fig. 6, the mixed state in Nb_3Al is paramagnetic. The $H_{C2}(T)$ from the Werthamer-Helfand-Hohenberg (WHH) theory,[16] which takes into account the effect of paramagnetic mixed state is given in a simplified form[17] as an implicit equation by

$$ln(t) = \psi\left[\frac{1}{2}\right] - \frac{1}{2}\left(1 + \frac{\lambda_{so}/4}{X}\right)\psi\left[\frac{1}{2} + \frac{Y + \lambda_{so}/4 - X}{t}\right] - \frac{1}{2}\left(1 - \frac{\lambda_{so}/4}{X}\right)\psi\left[\frac{1}{2} + \frac{Y + \lambda_{so}/4 + X}{t}\right], \quad (17)$$

where ψ is the digamma function and

$$Y = \frac{2h}{\pi^2}, \quad t = T/T_C, \quad (18a)$$

$$h = H_{C2}(T)/\left[\left(\frac{dH_{C2}}{dT}\right)_{T_C} T_C\right], \quad (18b)$$

$$X = \left[\left(\frac{\lambda_{so}}{4}\right)^2 - \frac{4h^2\alpha^2}{\pi^2}\right]^{1/2}, \quad (18c)$$

$$\alpha = \frac{\sqrt{2} \times 0.69(dH_{C2}/dT)_{T_C} T_C}{H_P(0)}, \quad (18d)$$

$$H_P(0) = 1.84 \times 10^4 T_C. \quad (18e)$$

Here $H_P(0)$ is the Chandrasekhar-Clogston limit of the upper critical field due to normal-state Pauli susceptibility and "α" is the Maki parameter which is related to the ratio of the orbital critical field and the Pauli-limited field. "λ_{so}" is the spin-orbit scattering parameter which gives relief from the Pauli limit of upper critical field.[16] For our case, the slope of upper critical field as a function of temperature at T_C, $(dH_{C2}/dT)_{T_C}$ is 29 500 Oe/K with T_C=17.1 K. The value of α turns out to be 1.564. In our earlier work[8] on the same sample, we had reported the T_C as nearly 16.8 K. Strictly speaking, that was the irreversibility temperature T_{irrv} and the actual T_C is slightly higher.

Figure 8 shows the experimentally determined $H_{C2}(T)$ along with the calculated $H_{C2}(T)$ using Eq. (17) for two extreme situations. The curve for the fully Pauli-limited H_{C2} is generated by taking λ_{so}=0 and the curve without Pauli limit is generated by taking λ_{so}=∞ (i.e., full relief from Pauli

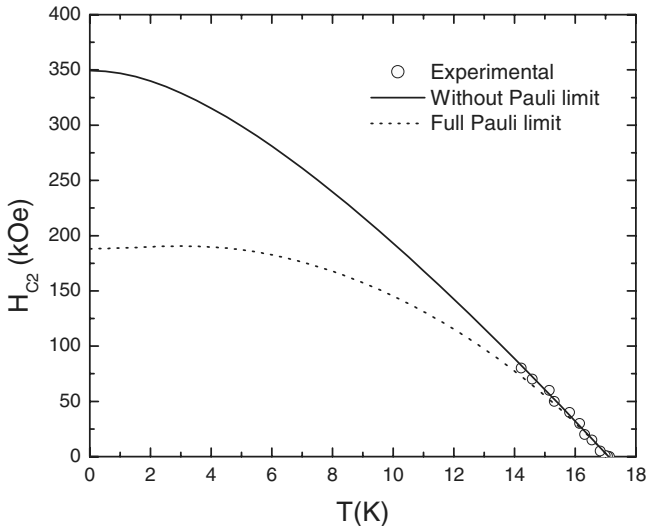

FIG. 8. Experimental H_{C2} as a function of T (open circles) along with the calculated curves using WHH theory [Eq. (17)]. The solid line is for the case without considering the Pauli limit while the dashed curve is for the case of fully Pauli-limited H_{C2}.

limit). We can see that the Pauli-limited curve severely underestimates the $H_{C2}(0)$, whereas the curve without the Pauli limit gives a slightly better fit to the experimental data. However, as discussed earlier in the context of Fig. 6, there is a significant paramagnetic susceptibility in the mixed state. Thus the curve generated from the WHH theory without taking into account the effect of paramagnetic mixed state is unphysical. A proper description of the H_{C2} of Nb_3Al thus requires a framework which includes the effect of strong electron-phonon and electron-electron correlations.[18] Such details are clearly beyond the scope of the work presented in this paper. Nevertheless, the curve generated from the WHH theory without considering the Pauli limit (Fig. 8) gives a reasonable estimate of the H_{C2} at zero temperature, which is about 350 kOe, and matches quite well with the experimentally observed H_{C2} in bulk samples.[13]

The coherence length at zero temperature $\xi(0)$ is estimated from the $H_{C2}(0)$ by

$$H_{C2}(0) = \frac{\Phi_0}{2\pi\xi(0)^2}, \tag{19}$$

where Φ_0 is the flux quantum and is approximately equal to 2.07×10^{-7} G cm^2. The coherence length $\xi(0)$ thus turns out to be almost 3 nm, which is nearly equal to the size of most of the grains [see Fig. 1(c)]. Some of the grains are actually smaller than this coherence length and can lead to various interesting superconducting properties.

The lower critical field H_{C1} at zero temperature is estimated by extrapolating the curve in the inset of Fig. 7 and is found to be almost 647 Oe. The penetration depth at zero temperature $\lambda(0)$ is given by

$$H_{C1}(0) = \frac{\Phi_0 \ln \kappa(0)}{4\pi\lambda(0)^2}, \tag{20}$$

where κ is the ratio of λ and ξ. $\lambda(0)$ turns out to be almost 94 nm, which is far larger than the largest of the superconducting grains. This indicates that the screening occurs as if the entire bulk sample is superconducting as we had noted during the discussion on Fig. 2.

Thus nanocrystalline superconductors can lead to a very interesting situation where the superconducting coherence length is nearly equal (or greater in some cases) to the typical grain size and the penetration depth is much larger than the largest of the grains. The work presented here shows that interesting applications such as the flow of bulk current through an assembly of nanoparticles is possible with the help of intermediate nonsuperconducting metallic matrix. Similar situation, but at much larger length scales has been studied in case of micrometer-sized Pb balls (ranging from few microns to a couple of tens of microns) separated by nonsuperconducting Al matrix.[19] A flow of bulk dissipationless current and bulk diamagnetism was observed even above the superconducting transition temperature of Al.[19] In our case, the situation becomes more interesting because the size of the superconducting grains themselves is on the order of ξ where the quantum limit on superconductivity sets in. Furthermore, as discussed in connection with Fig. 8, phenomena such as strong electron-phonon coupling and strong electron-electron correlations over a length scale of few lattice constants can provide interesting directions for future work.

IV. CONCLUSION

In conclusion we have measured the magnetization of nanocrystalline Nb_3Al as a function of magnetic field in the superconducting state. The isothermal magnetic hysteresis loop could be fitted by using the well-known Kim-Anderson model of critical state. The calculated field profiles using this model show a field variation over length scales much larger than the typical length scales of the superconducting grains. The fundamental length scales, the coherence length and the penetration depth, are estimated by analyzing the upper critical field and the lower critical field, respectively. The coherence length is found to be nearly the same as the typical grain size, whereas the penetration depth is found to be much larger than the size of the superconducting grains. Our results show that the proximity of nonsuperconducting metallic matrix to very-small-sized superconducting grains can provide a coupling between these grains for the flow of dissipationless current. It appears to be likely that the nonsuperconducting metallic matrix can overcome the quantum limit on the size of superconducting grains for the flow of lossless current. Interesting applications can arise in nanocrystalline superconductors, if the properties of the nonsuperconducting matrix along with the superconducting grains can be tuned properly.

*megh@rrcat.gov.in

[1] F.-Y. Wu, C. C. Yang, C.-M. Wu, C.-W. Wang, and W.-H. Li, J. Appl. Phys. **101**, 09G111 (2007).
[2] S. Bose, P. Raychaudhuri, R. Banerjee, P. Vasa, and P. Ayyub, Phys. Rev. Lett. **95**, 147003 (2005).
[3] S. Neeleshwar, Y. Y. Chen, C. R. Wang, M. N. Ou, and P. H. Huang, Physica C **408-410**, 209 (2004).
[4] C. T. Black, D. C. Ralph, and M. Tinkham, Phys. Rev. Lett. **76**, 688 (1996).
[5] H. J. Niu and D. P. Hampshire, Phys. Rev. B **69**, 174503 (2004).
[6] M. Tinkham, J. Supercond. Novel Magn. **13**, 801 (2000).
[7] A. Bezryadin, C. N. Lau, and M. Tinkham, Nature (London) **404**, 971 (2000).
[8] P. Mondal, M. Manekar, R. Kumar, T. Ganguli, and S. B. Roy, Appl. Phys. Lett. **92**, 052507 (2008).
[9] J. R. Clem and Z. Hao, Phys. Rev. B **48**, 13774 (1993).
[10] C.-Y. Wu, H.-M. Lin, H.-F. Lin, M.-F. Tai, C.-R. Wang, C.-K. Lin, and P. Y. Lee, Scr. Mater. **44**, 1967 (2001).
[11] A. Aharoni, J. Appl. Phys. **83**, 3432 (1998).
[12] J. L. Jorda, R. Flukiger, and J. Muller, J. Less-Common Met. **75**, 227 (1980).
[13] B. A. Glowacki, Intermetallics **7**, 117 (1999).
[14] D.-X. Chen and R. B. Goldfarb, J. Appl. Phys. **66**, 2489 (1989).
[15] T. P. Orlando and M. R. Beasley, Phys. Rev. Lett. **46**, 1598 (1981).
[16] N. R. Werthamer, E. Helfand, and P. C. Hohenberg, Phys. Rev. **147**, 295 (1966).
[17] T. P. Orlando, E. J. McNiff, Jr., S. Foner, and M. R. Beasley, Phys. Rev. B **19**, 4545 (1979).
[18] J. P. Carbotte, Rev. Mod. Phys. **62**, 1027 (1990).
[19] P. England, F. Goldie, and A. D. Caplin, J. Phys. F: Met. Phys. **17**, 447 (1987).